MULTIMODE SYNCHRONOUS RESONANCE DETECTION IN CONVERTER DOMINATED POWER SYSTEM USING SYNCHRO-WAVEFORMS

Taimur Zaman
University of Strathclyde, UK
Taimur.zaman@strath.ac.uk

Zhiwang Feng
University of Strathclyde, UK
zhiwang.feng@strath.ac.uk

Mazheruddin Syed
University of Strathclyde, UK
mazheruddin.syed@strath.ac.uk

Benedikt Pilscheur
Soraytec, Norway
b.pilscheur@soraytec.com

David Flynn
University of Glasgow, UK
david.flynn@glasgow.ac.uk

Graeme Burt
University of Strathclyde, UK
graeme.burt@strath.ac.uk

ABSTRACT

In recent years, the reporting of synchronous resonance events (sub-synchronous and super-synchronous) has become more common due to the rapid penetration of power grids with renewable power sources. The sub-synchronous events have been frequently observed for networks with wind farms connected downstream of the grid by-line compensators. However, new phenomena of multi-mode synchronous resonance have emerged due to the inverter-based resources (IBRs) interpolating range of frequencies in the fundamental frequency. Such events are significantly important to detect for stable operation of the system as the event results in escalating power oscillations in the network that can lead to the disconnection of generation sources and may damage the generators. Detection of such events using PMUs possess significant challenges in terms of their limited reporting rate, spectral leakage and picket fence effect, which intuitively report false amplitude and frequency of the modes of interest while detecting multimode resonance. Therefore, this work leverages novel synchro-waveforms to analyze the complex power sinusoids and initiate early detection of non-fundamental frequency intrusions in the signals leading to unstable operation and oscillation in the network. The proposed method is validated using the IEEE test benchmark and results demonstrate and support the potential real-time grid application.

INTRODUCTION

The consequent reporting of synchronous resonance events (sub-synchronous resonance subSR and super-synchronous resonance supSR) is one of the challenges that have become more common due to the rapidly evolving nature of power systems. The subSR events have been frequently observed due to the interaction between line compensators and power converters interfacing Distributed Energy Resources (DERs). Such events are more frequent in weak grids as shown in Fig.1, where reactive components are used for enhancing the power quality and compensating for the voltage regulations [1]. Apart from the conventional sub-synchronous resonance which primarily occurs due to the turbine generators and has only a single mode of oscillation, recent studies show that a distinct spectrum of oscillation may involve both sub-synchronous and super-synchronous resonance modes. For instance, the modes can be illustrated as one having a frequency above (50-100 Hz) and another below

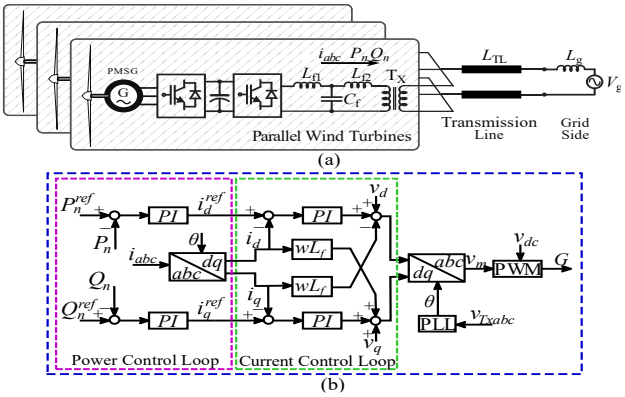

Fig.1. (a) Series compensated IBRs interfaced Grid, (b) Control System

(0.5-25Hz) the fundamental frequency (i.e., 50Hz). This phenomenon specifically stems from inverters-based power sources relying on asymmetrical dq control mechanisms [2]. Therefore, it is of great significance to detect all possible modes in the voltage/current profiles leading to power oscillations in the network.

The reporting rate limitation of phasor measurement units (PMUs) significantly degrades their capability to detect multimode synchronous resonance events. The events with frequency modes above the reporting rate and not qualifying the Nyquist critera causes spectral aliasing and inter-bin superimposition of respective frequency amplitudes. Therefore, the SubSR has a frequency mode well below the fundamental frequency of the system thus laying between 0.5 Hz to 25 Hz, however, modes with f_{SR} > 25 Hz tends significant challenges for its detection and require complex algorithams while using phasors based algorithms. Most of these methods are only able to detect single modes such as [3] and [4] uses DFT and compressive sensing, [5] use recursive least square based estimation and [6] report kalman filter based approach. The former approaches increases the computational complexity while constraints for optimal observability of all modes remain a question, whereas the later approaches require the preliminary information of f_{SR} to estimate; which is nonpractical for IBRs based systems.

The recently appeared Waveform Measurment Unitss (WMU) are a class of smart grid sensors enabling the time-synchronized measurement of voltage and current with the optimal sampling resolution that meets the minimum requirements of detecting any modes in SR, thus satisfying the Nyquist criteria [7]. The applications of the emerging technology can be found in detecting incipient faults in distribution grids [8] or detecting harmonics and classifying faults on a network under observation [9]. Further extending the application of time synchronized

WMU to detect the multimode SR in weak grids, this work proposes an online method to identify all modes in SR event escalating oscillations in the network. The proposed approach uses synchronized voltage and current waveforms typically available at the grid side and PCC of the compensators and IBRs-based sources. The proposed method is straightforward and leverages DFT based algorithm for extracting the fundamental and available modes in the power signal thus providing real-time monitoring of multimode SR frequencies.

The later section of the article explains how the multimode SR parameters are obtained by adaptively changing the window of DFT for voltage and currents obtained through Synchronized WMU. The performance of the algorithm is evaluated using sysnthetic signals and Matlab/Simulink simulations.

The remainder of the article is organized as folloes: Section (**II**) discusses the problem identification and phasors limitations in the event of multimode SR, while Section (**III**) provides insights on system description and Sliding DFT (SDFT) based approach for analyzing multimode SR using synchro-waveforms. The simulation results are provided in Section (**IV**) and the the work is concluded in Section (**V**).

PROBLEM IDENTIFICATION

Previously, resoance based oscillations have been frequently reported most of which are either forced or electromechanical oscillations. However, recently appeared complex and multimode resoance based oscillatioins are related to control interaction of IBRs and possess significant detection challenges for existing methods. Typically, the IBRs are synchronized and connected with grids following the *dq* transformation and control. The basic mechanism of *dq* transformation and its mathematical model is widely available in [3].

Recent studies identify that apart from the conventional SubSR which has typically $0<f<15$ Hz range, the SubSR is accompanied by SupSR having its frequency range $f>50$ Hz. This action is revealed from the frequency coupling incited due to dq transformation and reflects in the output voltage/current which triggers multimode oscillations [2].

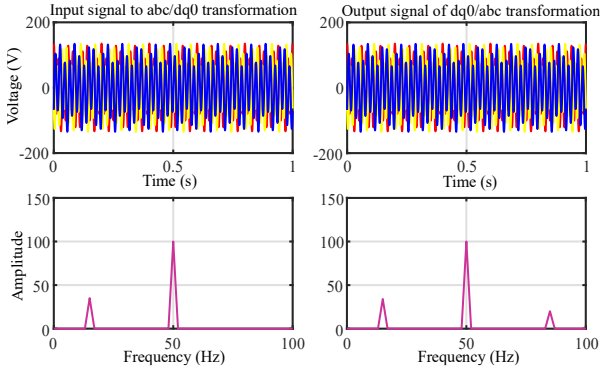

Fig.2. Multimode SR due to dq transformation

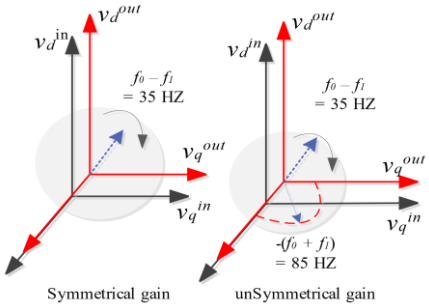

Fig. 3 Effect of symmetrical and asymmetrical gains in *dq*

To identify the root cause, a sinusoidal signal having two frequency components with 50 Hz as fundamental (f_o) and an extra frequency of 15 Hz is transformed into *dq* domain. For instance, the power signals considered can be expressed as follows,

$$\begin{aligned} v_a &= \sin(2\pi 50t) + 0.3\sin(2\pi 15t) \\ v_b &= \sin\left(2\pi\cdot 50t + \frac{2\pi}{3}\right) + 0.3\sin\left(2\pi\cdot 15t + \frac{2\pi}{3}\right) \\ v_c &= \sin\left(2\pi\cdot 50t - \frac{2\pi}{3}\right) + 0.3\sin\left(2\pi\cdot 15t - \frac{2\pi}{3}\right) \end{aligned} \quad (1)$$

The signal v_{abc} is transformed into dq reference frame using the Park and Clark transformation as shown in Fig.1b and provided in [4]. Fig. 2 shows typical output of abc/dq transformation providing same frequency contents as provided in (1) when *dq* gains are identical. However, the *dq* gains are asymetrical in practical applications as the grid and IBRs related constraints do not remain same. Therefore, the unequal *dq* vector with constituting frequency components split into two groups i.e., the fundamental frequency act as constant DC reference and 35Hz (= f_0-15) as rotating vector in the *dq* frame for first group while the negative frequency appears as second group of vectors rotating around the fundamental frequency = -(f_0 + *35*). On converting back to the three-phase domain, all the frequencies reflect in the output thus giving coupling of SubSR and SupSR leading to multimode resonance. This phenomenon is best illustrated in Fig.3 which is in alignment with Fig. 2 and illustrate the generated frequency. The reflected frequencies are computed in three phase domains as 15 Hz (i.e. -35 Hz + 50 Hz) and 85 Hz (i.e. 35 Hz + 50 Hz).

MATHEMATICAL ANALYSIS

Following up the preliminary discussion on frequency coupling inciting the multimode resonance that leads to low-frequency oscillations, the effect of multimode SR on fidelity of synchrophasors can be expressed by considering a sinusoidal signal having both subSR and supSR components as:

$$\begin{aligned} v[n] = A_0\cos(2\pi\frac{f_0}{N} + \\ \Phi_1)\sum_{i=1..2} A_i e^{\frac{\sigma_i}{N}n}.\cos(2\pi\frac{f_i}{N} + \Phi_i) \end{aligned} \quad (2)$$

where, the constants $A_0, A_i \ni [v_a[n] \quad v_b[n] \quad v_c[n]]^T$,

$$\mathring{S}[k,\gamma] = \underbrace{\left(\hat{A}_0 \cos\left(2\pi\frac{\Gamma_1}{f_0\cdot N}(k+\Gamma_0) + \Phi_0\right)e^{-j2\pi\frac{\gamma}{f_0}}\right)}_{\mathring{S}_{fo}[k,\Gamma]^{\mp}} + \underbrace{\frac{e^{\frac{k\sigma}{N}}}{f_i N}\left[\sum_{i=1}^{f_i-1}\left(A_i e^{\frac{\sigma_i}{N}i}\cos\left(2\pi\frac{\Gamma_i}{f_i\cdot N}(k+i) + \Phi_i\right)e^{-j2\pi\frac{\gamma i}{f_i}}\right)\right]}_{\mathring{S}_{sub/SR}[k,\Gamma]^{\mp}} \quad (5)$$

and are referred as amplitude of fundamental, multimode SR and positive sequence harmonics. Whereas, σ_i refers to the damping factor of the sample signal. The fundamental and subsequent frequency terms and phase are denoted as (f_0, f_1, f_2) & (Φ_1, Φ_2, Φ_3), respectively. Commonly $N \gg f_0$ to meet the Nyquist criteria for obtaining the required samples and hereby refers to the constant window length. Typically, the PMUs operate at 10-100 fps depending on the subject applications. Considering 100 fps for this work, the synchrophasors obtained through DFT with a fixed window length for fundamental frequency can be normalized as:

$$f_n = \frac{f_0}{N} \tag{3}$$

(3) can be written in terms of spectral bins and respective inter-bin frequency location as:

$$f_n = \sum_{i=0..j}^{j\neq 0} \frac{f_i}{N} = \frac{\Gamma_i}{N} \tag{4}$$

where Γ_i are the spectral bins of the frequencies in (2) and $= \Gamma_0 + ƀ_0$ specifically refers to the fundamental frequency spectral bin and inter bin location. Thus, the $\sum_{i=1..2} A_i e^{\frac{\sigma_i}{N}n} \cdot \cos(2\pi \cdot \frac{f_i}{N} + \Phi_i)$ have their respective spectral bins at $\pm\Gamma_i = \Gamma_i + ƀ_i$. From (5) for $f_i \neq f_0$, the spectral bins of corresponding synchrophasors are non-integers with $ƀ_i \neq 0 \therefore f_1 \in [\mathbf{0} \quad \mathbf{25}]$ & $f_2 \in [f_0 \quad f_0 \cdot \mathbf{n^{th}}] \Longrightarrow \Gamma_i \notin \mathbf{Z}^+$ and thus $v[n]$ has spectral leakage due to $\pm\Gamma_i$ not lying on integral bins. The spectrum of $v[n]$ for rectangular DFT window at the k^{th} sample can be written as (5).

From (5), k is the sample number and γ denotes the bin number. Further, (5) can be simplified based on Euler identity for $\cos(2\pi\frac{\Gamma_1}{N}(k+\Gamma_0)+\Phi_0)$ function reflecting the fundamental component in terms of its positive and negative spectrums and this can be written as (6).

Similarly, the multimode frequencies in terms of their

$$\mathring{S}_{fo}[\mathrm{k},\gamma]^{\mp} = \frac{1}{2Nf_0}\hat{A}_0\left[e^{j(2\pi\cdot k\cdot f_0+\Phi_0)}\forall_1(\Gamma_1-\gamma)+e^{-j(2\pi\cdot k\cdot f_0+\Phi_0)}\forall_1(\Gamma_1+\gamma)\right] \tag{6}$$

spectral bins can be interpreted as (7).

$$\mathring{S}_{f_\mathrm{i}}[\mathrm{k},\gamma]^{\mp} = \frac{1}{2\mathrm{N}*f_\mathrm{i}}A_i e^{\frac{\sigma_i}{N}\mathrm{i}}\left[\sum_{i=1}^{f_\mathrm{i}-1} e^{j(2\pi\cdot\mathrm{k}\cdot f_\mathrm{i}+\Phi_\mathrm{i})}\forall_\mathrm{i}(\Gamma_\mathrm{i}-\gamma_\mathrm{i}) + \mathrm{e}^{-j(2\pi\cdot\mathrm{k}\cdot f_\mathrm{i}+\Phi_\mathrm{i})}\forall_\mathrm{i}(\Gamma_\mathrm{i}+\gamma_\mathrm{i})\right] \tag{7}$$

Further, to facilitate the mathematical interpretation of (6) and (7), the spectral leakage can be denoted in terms of sampling requirements as:

$$\forall_1(\Gamma_1+\gamma) = \left\{\frac{1-e^{j2\pi(\Gamma_1+\gamma)}}{1-e^{j2\pi\left(\frac{\Gamma_1-\gamma}{\mathrm{N}f_0}\right)}}\right\} f_0 components \tag{8}$$

$$\forall_\mathrm{i}(\Gamma_\mathrm{i}+\gamma_\mathrm{i}) = \left\{\frac{1-e^{\left(\frac{\sigma_i}{N}\mathrm{i}+j2\pi(\Gamma_\mathrm{i}+\gamma_\mathrm{i})\right)}}{1-e^{\left(\frac{\sigma_i}{N}+j2\pi\frac{(\Gamma_\mathrm{i}+\gamma_\mathrm{i})}{\mathrm{N}\cdot f_\mathrm{i}}\right)}}\right\} f_\mathrm{i} \rightarrow f_{\mathrm{sub/sup}} \,||\, \mathrm{i} = 1,2.. \tag{9}$$

$$\mathring{S}[\mathrm{k},\gamma]^{+} = \Psi_1\hat{A}_0 e^{j(2\pi\cdot\mathrm{k}\cdot f_0+\Phi_0)} + \Psi_\mathrm{i}\sum_{i=1}^{f_\mathrm{i}-1} A_i e^{\frac{\sigma_i}{N}\mathrm{i}} e^{j(2\pi\cdot\mathrm{k}\cdot f_\mathrm{i}+\Phi_\mathrm{i})} \tag{10}$$

(9) & (10) fascilitate us in identifying the leakage factor terms and by solving for (5), we get:

$$\Psi_1 = \frac{1}{2\mathrm{N}f_0}\forall_1(\Gamma_1-\gamma) = \frac{1}{2\mathrm{N}f_0}\left[\frac{1-e^{j2\pi(\Gamma_1-\gamma)}}{1-e^{j2\pi\frac{(\Gamma_1-\gamma)}{\mathrm{N}\cdot f_0}}}\right. \tag{11}$$

$$\Psi_\mathrm{i} = \frac{1}{2\mathrm{N}*f_\mathrm{i}}\sum_{\mathrm{i}=1\ldots}\forall_\mathrm{i}(\Gamma_\mathrm{i}+\gamma_\mathrm{i}) = \frac{1}{2\mathrm{N}\cdot f_\mathrm{i}}\left[\frac{1-e^{\left(\frac{\sigma_i}{N}\mathrm{i}+j2\pi(\Gamma_\mathrm{i}+\gamma_\mathrm{i})\right)}}{1-e^{\left(\frac{\sigma_i}{N}+j2\pi\frac{(\Gamma_\mathrm{i}+\gamma_\mathrm{i})}{\mathrm{N}\cdot f_\mathrm{i}}\right)}}\right. \tag{12}$$

Considering that $f_n >> f_0$ for 50/60 Hz, there will be no spectral leakage for $\mathring{S}[\mathrm{k},\gamma]$ and only the positive spectrum can be considered as shown in (11). Fig. 3 & 4 confirms that for $f_n \approx f_0$ **v** $f_n \neq 2\cdot[f_{\mathrm{sub/sup}}]$, the Nyquist criteria for that specific band of frequencies doesn't satisfy, and therefore, spectral aliasing for that specific frequency band occurs on the negative spectral bins of the synchrophasor. This effects the reporting of correct frequency indices through PMUs thus leading to challenges associated with oscillations and other power quality problems.

Analysis using SDFT

For the extraction of signal over a set of frequencies of interest, the sliding discrete Fourier transform (SDFT) presents higher computation efficiency than the conventional fast Fourier transform (FFT) owing to its attribute for the signal spectrum being updated on a harmonic-by-harmonic basis [10]. Consequently, SDFT is employed in this paper to extract the signals with frequencies of interest from the voltage measurement. SDFT is initially deduced from the DFT circular shift property by multiplying the time domain sequence with $e^{j\frac{2\pi}{N}}$, which yields to

$$S_k(n) = e^{j\frac{2\pi k}{N}}[S_k(n-1)+x(n)-x(n-N)] \tag{13}$$

Applying the discretization to (13), the transfer function of SDFT can be derived as,

$$H_{\mathrm{SDFT}}(z) = \frac{S_k(n)}{x(n)} = (1-z^{-N})\frac{e^{j\frac{2\pi k}{N}}}{1-e^{j\frac{2\pi k}{N}}z^{-1}} \tag{14}$$

where N ($N=f_s/f_0$) is the window size, f_s is the sampling frequency, f_0 is the fundamental frequency, and k represents the frequency-domain signal spectrum index.

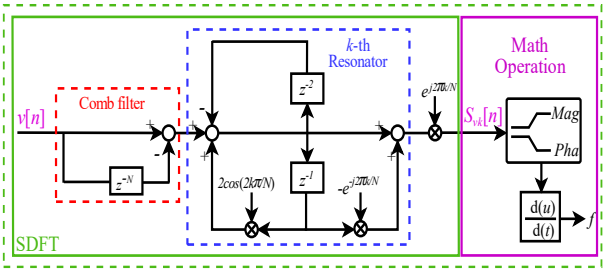

Fig.4. Comb filter based SDFT algorithm

To support the adoption of SDFT for power system

application in real-time with reduced computation complexity, the Geoertzel algorithm can be further applied to SDFT by multiplying the numerator and denominator of (14) with $1 - e^{j\frac{2\pi k}{N}}z^{-1}$ [10]. Consequently, the denominator of the modified SDFT comprises real-only coefficients and is given by

$$H_{\text{SDFT}}(z) = \underbrace{(1 - z^{-N})}_{\text{Comb filter}} \underbrace{\frac{\left(1 - e^{-j\frac{2\pi k}{N}}z^{-1}\right)e^{j\frac{2\pi k}{N}}}{1 - 2\cos\left(\frac{2k\pi}{N}\right)z^{-1} + z^{-2}}}_{\text{k-th complex resonator}} \quad (15)$$

As shown in Fig. 4, the SDFT filter can be envisioned as a comb filter cascading with multiple complex resonators. The complex resonator enables the selective amplification of the pre-attenuated signal component by the comb filter. Note that, the phase responses of the comb filter and complex resonator over the selective frequencies are zero as discussed in [11]. Correspondingly, the SDFT presents unity gain and zero phase response over the selective frequencies. This enables selective signal extraction from the original input signal without magnitude distortion and phase shift.

NUMERICAL VALIDATION

The proposed method is first validated using synthetic signals by constructing waveform using (2) in Matlab/Simulink and analyzed for different scenarios replicating the real-time sub/sup synchronous scenarios. The method is further evaluated using simulation studies by modeling a weak grid integrated with type 3 DFIG having a 5th order induction machine model. The induction machine is interfaced through a drive train model

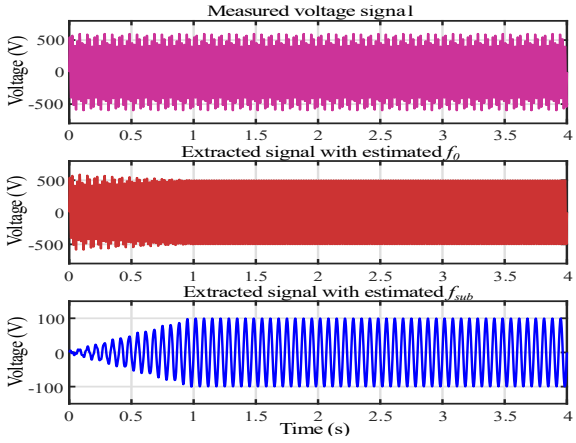

Fig.5 f_{sub} analysis using synthetic signals

representing the generator shaft. Mathematical models of GSC (Grid Side Converter) and RSC (Rotor Side Converter) are derived and their respective control parts are shown in Fig. 1b. The nominal frequency is 50 Hz with 128 data samples per cycle and simulation parameters are provided in Table I.

Fig.5a shows a voltage signal containing the subSR mode sampled at 7.2 kHz with random f_{sub} frequencies in the cyclic interval of the signal. Then, SDFT is used with 300 ms window that extract the fundamental component from

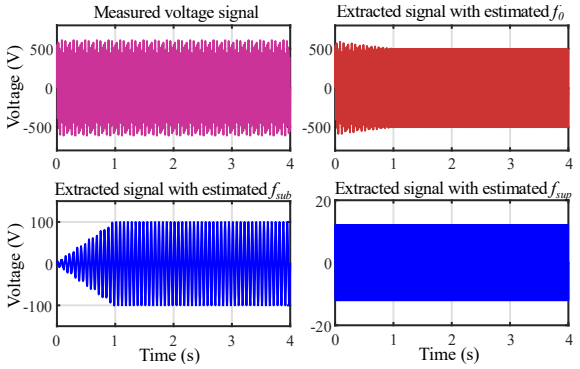

Fig.6 f_{sub} and f_{sup} analysis using synthetic signals

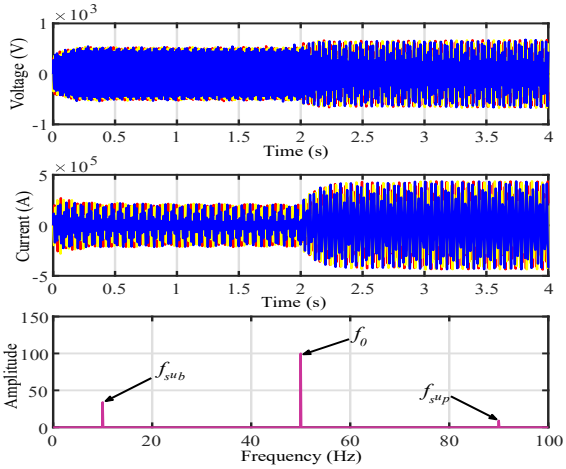

Fig.7. f_{sub} and f_{sup} analysis by varying control parameters

the multimode signal as shown in Fig.5b. This provides the primitive step for superimposing $A_0\cos(2\pi\frac{f_0}{N} + \Phi_1)$ over the extracted modes thus enabling us to estimate the sub/sup-SR components as shown in Fig. 5c.

To verify the concept of coupling frequencies emerging synchronous resonance with different modes, asymmetrical *dq* control is initiated as shown in Fig.6. The same sliding window (300ms) is applied across the measured voltage signal thus extracting f_0 from the orignal signal as shown in Fig.6a. The f_{sub} and f_{sup} are inferred from the measured voltage signal with frequencies and their respective magnitudes as 15Hz, 85Hz and 100V, 10V.

To verify the effectiveness of the proposed method for online estimation of modes in the SR based power signals, two test cases are conducted. The GSC part of the DFIG system controls the active and reactive power based on the reference generated from the PCC. Therefore, **i)** the GSC controls are asymmetrically increased leaving a minimum phase margin for its stability and can be well observed by deriving the transfer function for its control part. The wind speed is 11m/s and remains constant throughout the case. 25% extra line compensation is switched after 2 sec and its effect is illustrated in Fig.7. The asymmetry in control and extra compensation triggers the SR thus escalating oscillations in voltage and current waveforms. The SR can be hardly noticed in voltage waveforms till $t = 0 - 2$ *sec*, however noticeable oscillations appear in the current

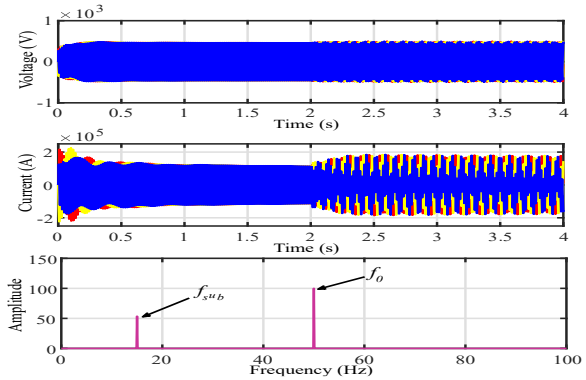

Fig.8. f_{sub} analysis by varying line compensation

waveforms after triggering extra compensation. Therefore, the SDFT with 600ms window infer the amplitdue of f_{sub} and f_{sup} frequencies by adjusting the SDFT resonator at ±50 Hz. The huge spikes in the current waveforms result due to 38% $|A_{sub}|$ and 9.8% $|A_{sup}|$ of the fundamental magnitude $|A_0|$ with f_{sub} =10 Hz and f_{sup} =90 Hz.

Similarly, **ii)** *In the second case,* the control gains are symmetric and the wind speed is 9m/s. This time, the multimode SR is not generated however the effect of subSR is obvious in the current waveform as shown in Fig. 8. The compensation level is not varied till *2 sec* and 15% variations are imposed onwards to see the effect. The SDFT reports the f_{sub} as 13Hz with 98.4% accuracy and amplitude 53% of the fundamental signal. This confirms another illustration that under balanced conditions, the grids are still vaulnerable to the SR based oscillations, however the affect is variations in compensations level.

The escalation of oscillation event in the voltage/current waveforms isn't intrinsic to be imitated as result of control or change in compensations, but can be induced as effect of fault in the system. The fault in the system can trigger both momentary or temporary oscillations and the damping depends on the location and type of fault. Similar case is investigated where three phase fault intrude the control symmetry and initiate the oscillations. Fault identification and characterization for oscillations escalation is another topic and beyond the scope of this work, however, using SDFT with pre-tuned resonators in subSR bandwidth allow us to identify the online cause of

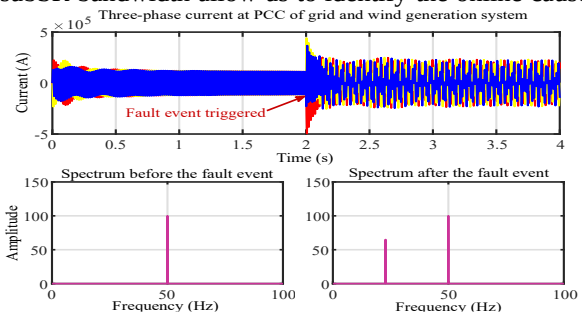

Fig.9 f_{sub} event due to symmetrical fault

oscillation event in the system as shown in Fig.9. This only takes 300ms window to identify the presence of SR modes in the current waveform for preliminary information regarding oscillations as shown in Fig.10b. The same window is applied after 2 sec and correctly determine the subSR mode with 99.1% accuracy.

CONCLUSION :

This paper proposed a unique method for online monitoring of multimode SR frequencies in IBRs interfaced weak grids connected through series compensated lines. The fidelity of synchronized phasors for such events is discussed and a synchrowaveforms-based online approach is proposed that leverages SDFT to extract modes from high sampled time domain signal. The estimated fundamental component and its amplitude are superimposed over-extracted modes to reconstruct the signal inducing oscillations. The effectiveness of the proposed method is validated by synthetic signals initially, while online monitoring is realized using Matlab/Simulink simulation. The proposed method has a great tendency for real-world applications and further research is recommended on the proposed approach to mitigate such challenges in a decentralized way.

TABLE I

SYSTEM PARAMETERS	
Transmission line (L_x,R_x)	0.4 H , 3.2Ω
Series capacitance, C	32μF
System voltage	161kV / 575V
Wind System Parameters	
Stator [Rs, Xs], Rotor [Rr, Xr]	[0.012 0.31] [0.015 0.28]
v_N , P_N , v_{DC}	500 V, 1.5MW, 1200 V
Control Parameters	
Kp_1, Kp_2, Kp_3, Kp_4,	[0.6 1 10 0.8]
Ki_1,Ki_2,Ki_2, Ki_3, Ki_4,	[20 3.2 08 13.5]

REFERENCES:

[1] F. Zhang, et al.,"Synchrophasors-Based Identification for Subsynchronous Oscillations in Power Systems," IEEE Trans. Smart Grid, vol. 10, no. 2, pp. 2224–2233, 2019.

[2] W. Ren et al.,"A Refined Frequency Scan Approach to Sub-Synchronous Control Interaction (SSCI) Study of Wind Farms," IEEE Trans. Power Syst., vol. 31, no. 5, pp. 3904–3912.

[3] K. Duda, et al.,"DFTbased Estimation of Damped Oscillation Parameters in Low-Frequency Mechanical Spectroscopy," IEEE Trans. Instrum. Meas., vol. 60, no. 11, pp. 3608–3618, 2011.

[4] C. Narduzzi et al.,"Fast-TFM—Multifrequency phasor measurement for distribution networks," IEEE Trans. Instrum. Meas., vol. 67, no. 8, pp. 1825–1835, 2018.

[5] Z. Ning, et al.,"Electromechanical Mode Online Estimation Using Regularized Robust RLS Methods," IEEE Trans. Power Syst., vol. 23, no. 4, pp. 1670–1680, 2008.

[6] T. Rajaram, et al.,"Kalman filter based detection and mitigation of subsynchronous resonance with SSSC," IEEE Trans. Power Syst., vol. 32, no. 2, pp. 1400–1409, Mar. 2017.

[7] M. Izadi and H. Mohsenian-Rad, "Event Location Identification in Distribution Networks Using Waveform Measurement Units," 2020 (ISGT-Europe), Netherlands, 2020, pp. 924-928

[8] M. Izadi et al.,"Synchronous Waveform Measurements to Locate Transient Events and Incipient Faults in Power Distribution Networks," IEEE Trans. Smart Grid, vol. 12, no. 5, 2021.

[9] D. M. Laverty et al.,"Time Synchronized Harmonic Analysis of Distribution Networks," 2022 IEEE Power & Energy Society General Meeting (PESGM), Denver, CO, USA, 2022, pp. 1-5.

[10] E. Jacobsen et al.,"The sliding DFT," in IEEE Signal Processing Magazine, vol. 20, no. 2, pp. 74-80, March 2003.

[11] Z. Feng et al.,"A Scheme to Improve the Stability and Accuracy of Power Hardware-in-the-Loop Simulation," IECON 2020 The 46th Annual Conference of the IEEE Ind. Electronics Society, 2020.